

Contrastive Similarity Matching for Supervised Learning

Shanshan Qin¹, Nayantara Mudur², and Cengiz Pehlevan¹

¹John A. Paulson School of Engineering and Applied Sciences,
Harvard University, Cambridge, MA USA

²Department of Physics, Harvard University, Cambridge, MA USA

Abstract

We propose a novel biologically-plausible solution to the credit assignment problem, being motivated by observations in the ventral visual pathway and trained deep neural networks. In both, representations of objects in the same category become progressively more similar, while objects belonging to different categories becomes less similar. We use this observation to motivate a layer-specific learning goal in a deep network: each layer aims to learn a representational similarity matrix that interpolates between previous and later layers. We formulate this idea using a contrastive similarity matching objective function and derive from it deep neural networks with feedforward, lateral and feedback connections, and neurons that exhibit biologically-plausible Hebbian and anti-Hebbian plasticity. Contrastive similarity matching can be interpreted as an energy-based learning algorithm, but with significant differences from others in how a contrastive function is constructed.

1 Introduction

Synaptic plasticity is generally accepted to be the underlying mechanism of learning in the brain, which almost always involves a large population of neurons and synapses across many different brain regions. How the brain modifies and coordinates individual synapses in the face of limited information available to each synapse in order to achieve a global learning task, the credit assignment problem, has puzzled scientists for decades. A major effort in this domain has been to look for a biologically-plausible implementation of the back-propagation of error algorithm (BP) (Rumelhart et al., 1986), which has long been disputed due to its

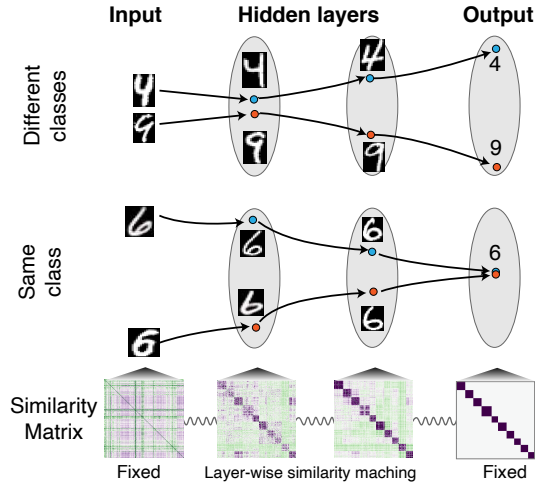


Figure 1: Supervised learning via layer-wise similarity matching. For inputs of different categories, similarity-matching differentiates the representations progressively (up), while for objects of the same category, representations become more and more similar (middle). For a given set of training data and their corresponding labels, the training process can be regarded as learning hidden representations whose similarity matrices match that of both input and output (lower). The tuning of representational similarity is indicated by the springs with the constraints that input and output similarity matrices are fixed.

biologically implausibility (Crick, 1989), although recent work has made progress in resolving some of these concerns (Xie and Seung, 2003; Lee et al., 2015; Lillicrap et al., 2016; Nøkland, 2016; Scellier and Bengio, 2017; Guerguiev et al., 2017; Whittington and Bogacz, 2017; Sacramento et al., 2018; Richards and Lillicrap, 2019; Whittington and Bogacz, 2019; Belilovsky et al., 2018; Ororbia and Mali, 2019; Lillicrap et al., 2020).

In this paper, we present a novel approach to the credit assignment problem, motivated by observations on the nature of hidden layer representations in the ventral visual pathway of the brain and deep neural networks. In both, representations of objects belonging to different categories become less similar, while same category become more similar (Grill-Spector and Weiner, 2014). In other words, categorical clustering of representations becomes more and more explicit at the later layers (Fig. 1). These results suggest a new approach to the credit assignment problem. By assigning each layer a layer-local similarity matching task (Pehlevan and Chklovskii, 2019), whose goal is to learn an intermediate representational similarity matrix between previous and later layers, we may be able to get away from the need of backward propagation of errors (Fig. 1). Motivated by this idea and previous observations that error signal can be implicitly

propagated via the change of neural activities (Hinton and McClelland, 1988; Scellier and Bengio, 2017), we propose a contrastive similarity matching objective function and derive from it deep neural networks with feedforward, lateral and feedback connections, and neurons that exhibit biologically-plausible Hebbian and anti-Hebbian plasticity.

We first derive a neural network that serves as the backbone for biologically plausible supervised learning from an objective which we term “Supervised Similarity Matching” (SSM). The supervised signal is introduced to the network by clamping the output neurons to the desired states. The hidden layers learn intermediate representations between their previous and later layers by optimizing a layer-local similarity matching objective function. Optimizing a dual minimax formulation of this problem by an alternating gradient ascent-descent (Pehlevan et al., 2018) leads to the operation of a neural network with local Hebbian learning rules for the feedforward and feedback weights, and anti-Hebbian learning rules for the lateral weights of the hidden layers.

We then introduce the contrastive similarity matching objective by adding a nudging term to SSM, from which we derive a biologically plausible learning algorithm, the Contrastive Similarity Matching (CSM) algorithm. Our approach is similar to energy-based learning algorithms such as Contrastive Hebbian Learning (CHL) (Movellan, 1991) and Equilibrium Propagation (EP) (Scellier and Bengio, 2017), where weight-updates rely on the difference of the neural activity between a free phase, and a clamped” (CHL) or “nudged (EP) phase to locally approximate the gradient of an error signal. The learning process can be interpreted as minimizing a contrastive function, which reshapes the energy landscape to eliminate spurious fixed points and makes the desired fixed point more stable.

The CSM algorithm is derived from the same duality principles as before, which has two-phases. The first phase is analogous to the nudged phase of EP, and performs Hebbian feedforward and anti-Hebbian lateral updates. We emphasize that our algorithm has the opposite sign for the lateral connection updates compared with EP and CHL. This is due to the fact that our weight updates solve a minimax problem. Anti-Hebbian learning pushes each neuron within a layer to learn different representations. In the second phase of our algorithm, only the feedforward weights are updated by anti-Hebbian rule. This is again different from EP or CHL where all weights are updated.

Our main contributions and results are listed below:

- We introduce a novel approach to the credit assignment problem using biologically-plausible learning rules. We introduce the Contrastive Similarity Matching algorithm. Our work generalizes the similarity matching principle (Pehlevan and Chklovskii, 2019) to supervised learning tasks.
- The proposed supervised learning algorithms can be related to other energy-

based algorithms, but with distinct underlying mechanism.

- We present a version of our neural network algorithm with structured connectivity.
- Using numerical simulations, we show that the performance of our algorithms is on par with other energy-based algorithms. The learned representations of our Hebbian/anti-Hebbian network is more sparse and structured.

The rest of this paper is organized as follows. In Section 2, we derive linear neural network for linear supervised tasks based on the Supervised Similarity Matching objective. In Section 3, we present the Contrastive Similarity Matching algorithm for deep neural networks with nonlinear activation functions and structured connectivity. We discuss the relation of our algorithm to other energy-based learning algorithms. In Section 4, we report the performance of our algorithm and compare it with EP, highlighting the differences between them. Finally, we discuss our results and relate it to other works in Section 5.

2 Supervised Similarity Matching for Linear Tasks

We start by deriving a neural network (NN) that solves deterministic and noisy linear tasks based on the similarity matching principle. Our approach is normative, in the sense that we derive an online algorithm by optimizing an objective function, and map the steps of the algorithm onto the operation of a biologically-plausible neural network. In contrast to conventional deep learning approaches, the neural architecture and dynamics are not prescribed but derived from the optimization problem.

Our goal in this section is to introduce some of the key ideas behind the development of the Contrastive Similarity Matching algorithm. Therefore, we will focus on the simplest non-trivial NN architecture, a NN with a single hidden layer and linear activation functions.

2.1 Supervised Similarity Matching Objective

Let $\mathbf{x}_t \in \mathbb{R}^n$, $t = 1, \dots, T$ be a set of data points and $\mathbf{z}_t^l = \mathbf{A}\mathbf{x}_t$, where $\mathbf{z}_t^l \in \mathbb{R}^k$, $\mathbf{A} \in \mathbb{R}^{k \times n}$, $k \leq n$, be their corresponding desired output or labels. Our goal is to derive a NN with one hidden layer that uses biologically plausible learning rules to learn the underlying linear function between \mathbf{x} and \mathbf{z} . As we will see below, \mathbf{x} will be the inputs to a neural network and \mathbf{z}^l will be the outputs.

Our idea is that the representation learned by the hidden layer, $\mathbf{y} \in \mathbb{R}^m$, should be half-way between the input \mathbf{x} and the desired output \mathbf{z}^l . We formulate this

idea using representational similarities, quantified by the dot product of representational vectors within a layer. Our proposal can be formulated as the following optimization problem:

$$\min_{\{\mathbf{y}_t\}_{t=1}^T} \frac{1}{T^2} \sum_{t=1}^T \sum_{t'=1}^T [(\mathbf{x}_t^\top \mathbf{x}_{t'} - \mathbf{y}_t^\top \mathbf{y}_{t'})^2 + (\mathbf{y}_t^\top \mathbf{y}_{t'} - \mathbf{z}_t^{l\top} \mathbf{z}_{t'}^l)^2]. \quad (1)$$

To get an intuition about what this cost function achieves, consider the case where only one training datum exists. Then, $\mathbf{y}_1^\top \mathbf{y}_1 = \frac{1}{2}(\mathbf{x}_1^\top \mathbf{x}_1 + \mathbf{z}_1^{l\top} \mathbf{z}_1^l)$, satisfying our condition. When multiple training data are involved, interactions between different data points lead to a non-trivial solution, but the fact that the hidden layer representations are in between the input and output layers stays.

The optimization problem (1) can be analytically solved, making our intuition precise. Let the representational similarity matrix of the input layer be $R_{tt'}^x \equiv \mathbf{x}_t^\top \mathbf{x}_{t'}$, the hidden layer be $R_{tt'}^y \equiv \mathbf{y}_t^\top \mathbf{y}_{t'}$, and the output layer be $R_{tt'}^z \equiv \mathbf{z}_t^{l\top} \mathbf{z}_{t'}^l$. Instead of solving for \mathbf{y} directly, we can reformulate and solve the supervised similarity matching problem (1) for \mathbf{R}^y , and then obtain \mathbf{y} s by a matrix factorization through an eigenvalue decomposition. By completing square, problem (1) becomes an optimization problem for \mathbf{R}^y :

$$\min_{\mathbf{R}^y \in \mathcal{S}^m} \frac{1}{T^2} \left\| \frac{1}{2} (\mathbf{R}^x + \mathbf{R}^z) - \mathbf{R}^y \right\|_F^2, \quad (2)$$

where \mathcal{S}^m is the set of symmetric matrices with rank m , and F denotes the Frobenious norm. Optimal \mathbf{R}^y is given by keeping the top m modes in the eigenvalue decomposition of $\frac{1}{2} (\mathbf{R}^x + \mathbf{R}^z)$ and setting the rest to zero. If $m \geq \text{rank}(\mathbf{R}^x + \mathbf{R}^z)$, then optimal \mathbf{R}^y exactly equals $\frac{1}{2} (\mathbf{R}^x + \mathbf{R}^z)$, achieving a representational similarity matrix that is the average of input and output layers.

2.2 Derivation of a Supervised Similarity Matching Neural Network

The supervised similarity matching cost function (1) is formulated in terms of the activities of units, but a statement about the architecture and the dynamics of the network has not been made. In fact, we will derive all these from the cost function, without prescribing them. To do so, we need to introduce variables that correspond to the synaptic weights in the network. As it turns out, these variables are dual to correlations between unit activities (Pehlevan et al., 2018).

To see this explicitly, following the method of (Pehlevan et al., 2018), we expand the squares in Eq.(1) and introduce new dual variables $\mathbf{W}_1 \in \mathbb{R}^{m \times n}$,

$\mathbf{W}_2 \in \mathbb{R}^{k \times m}$ and $\mathbf{L}_1 \in \mathbb{R}^{m \times m}$ using the following identities:

$$\begin{aligned}
-\frac{1}{T^2} \sum_{t=1}^T \sum_{t'=1}^T \mathbf{y}_t^\top \mathbf{y}_{t'} \mathbf{x}_t^\top \mathbf{x}_{t'} &= \min_{\mathbf{W}_1} -\frac{2}{T} \sum_{t=1}^T \mathbf{y}_t^\top \mathbf{W}_1 \mathbf{x}_t + \text{Tr} \mathbf{W}_1^\top \mathbf{W}_1, \\
\frac{1}{T^2} \sum_{t=1}^T \sum_{t'=1}^T \mathbf{y}_t^\top \mathbf{y}_{t'} \mathbf{y}_t^\top \mathbf{y}_{t'} &= \max_{\mathbf{L}_1} \frac{2}{T} \sum_{t=1}^T \mathbf{y}_t^\top \mathbf{L}_1 \mathbf{y}_t - \text{Tr} \mathbf{L}_1^\top \mathbf{L}_1, \\
-\frac{1}{T^2} \sum_{t=1}^T \sum_{t'=1}^T \mathbf{y}_t^\top \mathbf{y}_{t'} \mathbf{z}_t^{l\top} \mathbf{z}_{t'}^l &= \min_{\mathbf{W}_2} -\frac{2}{T} \sum_{t=1}^T \mathbf{z}_t^{l\top} \mathbf{W}_2 \mathbf{y}_t + \text{Tr} \mathbf{W}_2^\top \mathbf{W}_2.
\end{aligned} \tag{3}$$

Plugging these into Eq.(1), and changing orders of optimization, we arrive the following dual, minimax formulation of supervised similarity matching:

$$\min_{\mathbf{W}_1, \mathbf{W}_2} \max_{\mathbf{L}_1} \frac{1}{T} \sum_{t=1}^T l_t(\mathbf{W}_1, \mathbf{W}_2, \mathbf{L}_1, \mathbf{x}_t, \mathbf{z}_t^l), \tag{4}$$

where

$$\begin{aligned}
l_t &:= \text{Tr} \mathbf{W}_1^\top \mathbf{W}_1 - \text{Tr} \mathbf{L}_1^\top \mathbf{L}_1 + \text{Tr} \mathbf{W}_2^\top \mathbf{W}_2 \\
&+ \min_{\mathbf{y}_t} 2(-\mathbf{y}_t^\top \mathbf{W}_1 \mathbf{x}_t + \mathbf{y}_t^\top \mathbf{L}_1 \mathbf{y}_t - \mathbf{y}_t^\top \mathbf{W}_2^\top \mathbf{z}_t^l).
\end{aligned} \tag{5}$$

A stochastic optimization of the above objective can be mapped to a Hebbian/anti-Hebbian network following steps in previous work (Pehlevan et al., 2018). For each training datum, $\{\mathbf{x}_t, \mathbf{z}_t^l\}$, a two-step procedure is performed. First, optimal \mathbf{y}_t that minimizes l_t is obtained by a gradient flow until convergence,

$$\dot{\mathbf{y}} = \mathbf{W}_1 \mathbf{x}_t - 2\mathbf{L}_1 \mathbf{y}_t + \mathbf{W}_2^\top \mathbf{z}_t^l. \tag{6}$$

We interpret this flow as the dynamics of a neural circuit with linear activation functions, where the dual variables $\mathbf{W}_1, \mathbf{W}_2$ and \mathbf{L}_1 are synaptic weight matrices (Fig. 2A). In the second part of the algorithm, we update the synaptic weights by a gradient descent-ascent on (5) with \mathbf{y}_t fixed. This gives the following synaptic plasticity rules

$$\Delta \mathbf{W}_1 = \eta(\mathbf{y}_t \mathbf{x}_t^\top - \mathbf{W}_1), \quad \Delta \mathbf{L}_1 = \eta(\mathbf{y}_t \mathbf{y}_t^\top - \mathbf{L}_1), \quad \Delta \mathbf{W}_2 = \eta(\mathbf{z}_t^l \mathbf{y}_t^\top - \mathbf{W}_2). \tag{7}$$

The learning rate η of each matrix can be chosen differently to achieve best performance.

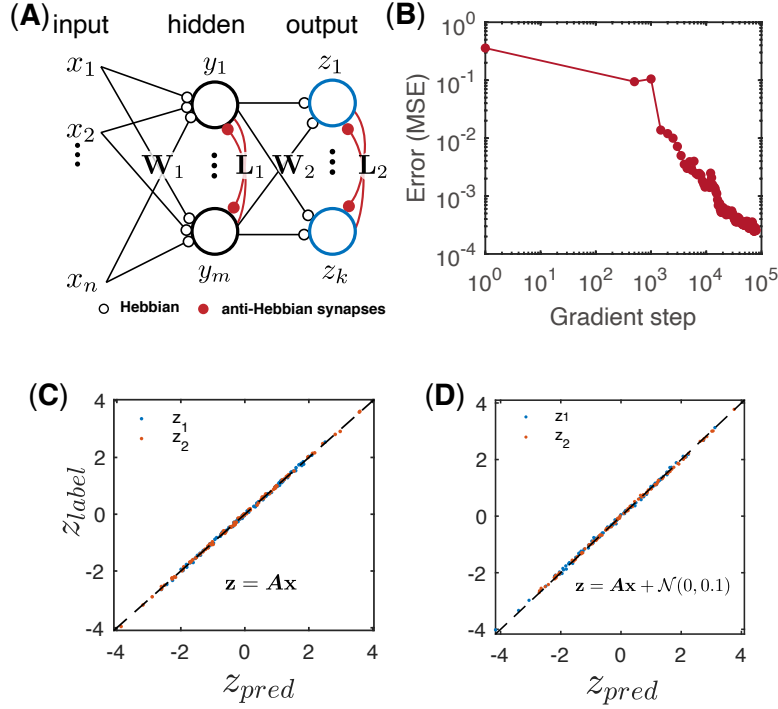


Figure 2: A linear NN with Hebbian/anti-Hebbian learning rules. (A) During the learning process, the output neurons (blue) are clamped at their desired states. After training, prediction for a new input \mathbf{x} is given by the value of \mathbf{z} at the fixed point of neural dynamics. (B) Test error, defined as the mean square error between the network’s prediction, \mathbf{z}_t^p , and the ground-truth value, \mathbf{z}_t^l , $1/T \sum_{t=1}^T \|\mathbf{z}_t^p - \mathbf{z}_t^l\|_F^2$, decreases with the gradient ascent-descent steps during learning. (C) Scatter plot of the predicted value versus the desired value (element-wise). (D) The algorithm learns the correct mapping between \mathbf{x} and \mathbf{z} even in the presence of Gaussian noise. In these examples, $\mathbf{x} \in \mathbb{R}^5$, $\mathbf{A} \in \mathbb{R}^{2 \times 5}$, elements of \mathbf{x} and \mathbf{A} are drawn from a uniform distribution in the range $[-1, 1]$, $\mathbf{y} \in \mathbb{R}^2$ and $\mathbf{z} \in \mathbb{R}^2$. In (C) and (D), 200 data points are shown.

Overall, the network dynamics (6) and the update rules (7) map to a NN with one hidden layer, with the output layer clamped to the desired state. The updates of the feedforward weight are Hebbian, and updates of the lateral weight are “anti-Hebbian” since the \mathbf{L}_1 connections are inhibitory (Fig. 2A).

For prediction, the network takes an input data point, \mathbf{x}_t , and runs with unclamped output until convergence. We take the value of the \mathbf{z} units at the fixed point as the network’s prediction.

To make sure that the network produces correct fixed points, at least for training data, we introduce the following step to the training procedure. We aim to construct a neural dynamics for the output layer in prediction phase such

that its fixed point \mathbf{z} corresponds to the desired output \mathbf{z}^l . Since the output layer receives input $\mathbf{W}_2\mathbf{y}$ from previous layer, a decay term that depends on \mathbf{z} is required to achieve stable fixed point at $\mathbf{z} = \mathbf{z}^l$. The simplest way is introducing lateral inhibitions. And now the output layer has the following neural dynamics:

$$\dot{\mathbf{z}} = \mathbf{W}_2\mathbf{y} - \mathbf{L}_2\mathbf{z}, \quad (8)$$

where the lateral connections \mathbf{L}_2 are learned such that the fixed point $\mathbf{z}^* \approx \mathbf{z}^l$. This is achieved by minimizing the following target function

$$\min_{\mathbf{L}_2} \frac{1}{T} \sum_{t=1}^T \|\mathbf{W}_2\mathbf{y}_t - \mathbf{L}_2\mathbf{z}_t^l\|_2^2. \quad (9)$$

Taking the derivative of the above target function with respect to \mathbf{L}_2 while keeping other parameters and variables evaluated at the fixed point of neural dynamics, we get the following “delta” learning rule for \mathbf{L}_2 :

$$\Delta\mathbf{L}_2 = \eta(\mathbf{W}_2\mathbf{y}_t - \mathbf{L}_2\mathbf{z}_t^l)\mathbf{z}_t^{l\top}. \quad (10)$$

After learning, the NN makes a prediction about a new input \mathbf{x} by running the neural dynamics of \mathbf{y} and \mathbf{z} (6) and (8) until they converge to a fixed point. We take the value of \mathbf{z} units at the fixed point as the prediction. As shown in Fig.2 B-D, the linear network and weight update rule solve linear tasks efficiently.

Although the above procedure can be generalized to multi-layer and nonlinear networks, one has to address the issue of spurious fixed points of nonlinear dynamics for a given input \mathbf{x}_t . To overcome this problem, we will introduce the Contrastive Similarity Matching algorithm, borrowing ideas from energy-based learning algorithms such as Contrastive Hebbian Learning (CHL) and Equilibrium Propagation (EP) in the next section.

3 Contrastive Similarity Matching for Deep Non-linear Networks

In energy-based learning algorithms like CHL and EP, weight updates rely on the difference of neural activity between a free phase and a clamped/nudged phase to locally approximate the gradient of an error signal. This process can be interpreted as minimizing a contrastive function, which reshapes the energy landscape to eliminate the spurious fixed points and make the fixed point corresponding to the desired output more stable.

We will adopt this idea to derive the Contrastive Similarity Matching algorithm. In order to do so, we will first introduce what we call the “nudged similarity matching” cost function, and derive its dual formulation, which will be the energy function used in our contrastive formulation.

3.1 Nudged Deep Similarity Matching Objective and Its Dual Formulation

We now discuss a P -layer ($P - 1$ hidden layers) NN with nonlinear activation functions, f . For notational convenience, we denote inputs to the network by $\mathbf{r}^{(0)}$, outputs by $\mathbf{r}^{(P)}$, and activities of hidden layer units by $\mathbf{r}^{(p)}$, $p = 1, \dots, P - 1$.

We propose the following objective function for the training phase where outputs are nudged towards the desired labels

$$\begin{aligned} \min_{\substack{a_1 \leq \mathbf{r}_t^{(p)} \leq a_2 \\ t=1, \dots, T \\ p=1, \dots, P}} \sum_{p=1}^P \frac{\gamma^{p-P}}{2T^2} \sum_{t=1}^T \sum_{t'=1}^T \|\mathbf{r}_t^{(p-1)\top} \mathbf{r}_{t'}^{(p-1)} - \mathbf{r}_t^{(p)\top} \mathbf{r}_{t'}^{(p)}\|_2^2 + \sum_{p=1}^P \frac{2\gamma^{p-P}}{T} \sum_{t=1}^T \mathbf{F}(\mathbf{r}_t^{(p)})^\top \mathbf{1} \\ + \frac{\beta}{T} \sum_{t=1}^T \|\mathbf{r}_t^{(P)} - \mathbf{z}_t^l\|_2^2, \end{aligned} \quad (11)$$

where β is a control parameter that specifies how strong the nudge is, $\gamma \geq 0$ is a parameter that allows the influence of the later layers to the previous layers, $F(\mathbf{r}_t^{(p)})$ is a regularizer defined and related to the activation function by $dF(\mathbf{r}_t^{(p)})/d\mathbf{r}_t^{(p)} = \mathbf{u}_t^{(p)} - \mathbf{b}_t^{(p)}$, where $\mathbf{r}_t^{(p)} = f(\mathbf{u}_t^{(p)})$, $\mathbf{u}_t^{(p)}$ and $\mathbf{r}_t^{(p)}$ are the total input and output of p -th layer respectively, $\mathbf{b}_t^{(p)}$ is the threshold of neurons in layer p . We also assume f to be a monotonic and bounded function, whose bounds are given by a_1 and a_2 .

The objective function (11) is almost identical to the deep similarity matching objective that was introduced in (Obeid et al., 2019), except the nudging term. Obeid et al. (2019) used $\beta = 0$ version as an unsupervised algorithm. Here, we use a non-zero β for supervised learning.

Using analogues of the duality transforms discussed in the previous section and in (Pehlevan et al., 2018; Obeid et al., 2019), the above nudged supervised deep similarity matching problem (11) can be turned into a minimax problem:

$$\min_{\{\mathbf{W}^{(p)}\}} \max_{\{\mathbf{L}^{(p)}\}} \frac{1}{T} \sum_{t=1}^T l_t \left(\{\mathbf{W}^{(p)}\}, \{\mathbf{L}^{(p)}\}, \mathbf{r}_t^{(0)}, \mathbf{z}_t^l, \beta \right), \quad (12)$$

where

$$\begin{aligned} l_t := \min_{\substack{a_1 \leq \mathbf{r}_t^{(p)} \leq a_2 \\ p=1, \dots, P}} \sum_{p=1}^P \gamma^{p-P} \left[\text{Tr} \mathbf{W}^{(p)\top} \mathbf{W}^{(p)} - 2\mathbf{r}_t^{(p)\top} \mathbf{W}^{(p)} \mathbf{r}_t^{(p-1)} \right. \\ \left. + \frac{1 + \gamma(1 - \delta_{pP})}{2} c^{(p)} \left(2\mathbf{r}_t^{(p)\top} \mathbf{L}^{(p)} \mathbf{r}_t^{(p)} - \text{Tr} \mathbf{L}^{(p)\top} \mathbf{L}^{(p)} \right) + 2\mathbf{F}(\mathbf{r}_t^{(p)})^\top \mathbf{1} \right] + \beta \|\mathbf{r}_t^{(P)} - \mathbf{z}_t^l\|_2^2, \end{aligned} \quad (13)$$

where we introduced $c^{(p)}$ as a parameter that governs the relative importance of forward versus recurrent inputs and $c^{(p)} = 1$ corresponds to the exact transformation, details of which is given in the Appendix A.

We note that the objective of the min in l_t defines an energy function for a NN. It can be minimized by running the following dynamics:

$$\begin{aligned}\tau_p \frac{d\mathbf{u}^{(p)}}{dt} &= -\mathbf{u}^{(p)} + \mathbf{W}^{(p)} \mathbf{r}_t^{(p-1)} - c^{(p)} [1 + \gamma(1 - \delta_{pP})] \mathbf{L}^{(p)} \mathbf{r}_t^{(p)} + \mathbf{b}_t^{(p)} \\ &\quad + \gamma(1 - \delta_{pP}) \mathbf{W}^{(p+1)\top} \mathbf{r}_t^{(p+1)} - \beta \delta_{pP} (\mathbf{r}_t^{(P)} - \mathbf{z}_t^l), \\ \mathbf{r}_t^{(p)} &= \mathbf{f}(\mathbf{u}^{(p)}),\end{aligned}\tag{14}$$

where δ_{pP} is the Kronecker delta, $p = 1, \dots, P$, τ_p is a time constant, $\mathbf{W}^{(P+1)} = \mathbf{0}$, $\mathbf{r}_t^{(P+1)} = \mathbf{0}$. This observation will be the building block of our CSM algorithm, which we present below.

3.2 Contrastive Similarity Matching

We first state our contrastive function and then discuss its implications. We suppress the dependence on training data in l_t and define:

$$\{\mathbf{L}^{*(p)}\} \equiv \arg \max_{\{\mathbf{L}^{(p)}\}} \frac{1}{T} \sum_{t=1}^T l_t(\{\mathbf{W}^{(p)}\}, \{\mathbf{L}^{(p)}\}, \{\mathbf{b}^{(p)}\}, \beta),\tag{15}$$

and

$$E(\{\mathbf{W}^{(p)}\}, \{\mathbf{b}^{(p)}\}, \beta) = \frac{1}{T} \sum_{t=1}^T l_t(\{\mathbf{W}^{(p)}\}, \{\mathbf{L}^{*(p)}\}, \{\mathbf{b}^{(p)}\}, \beta).\tag{16}$$

Finally, we formulate our contrastive function as

$$J^\beta(\{\mathbf{W}^{(p)}\}, \{\mathbf{b}^{(p)}\}) = E(\beta) - E(0),\tag{17}$$

which is to be minimized over feedforward and feedback weights $\{\mathbf{W}^{(p)}\}$, as well as bias $\{\mathbf{b}^{(p)}\}$. For fixed bias, minimization of the first term, $E(\beta)$ corresponds exactly to the optimization of the minimax dual of nudged deep similarity matching (12). The second term $E(0)$ corresponds to a free phase, where no nudging is applied. We note that in order to arrive at a contrastive minimization problem, we use the same optimal lateral weights, (15), from the nudged phase in the free phase. Compared to the minimax dual of nudged deep similarity matching (12), we also optimize over the bias for better performance.

Minimization of the contrastive function (17) closes the energy gap between nudged and free phases. Because the energy functions are evaluated at the fixed

Algorithm 1 Constrative Similarity Matching (CSM)

Input: Initial $\{\mathbf{W}^{(p)}\}, \{\mathbf{L}^{(p)}\}, \{\mathbf{b}^{(p)}\}, \{\mathbf{r}^{(p)}\}$
for $t = 1$ **to** T **do**
 Run the nudged phase neural dynamics (14) with $\beta \neq 0$ until convergence,
 collect the fixed point $\{\mathbf{r}_{\beta,t}^{(p)}\}$
 Run the free phase dynamics (14) with $\beta = 0$ until convergence, collect fixed
 point $\{\mathbf{r}_{0,t}^{(p)}\}$
 Update $\{\mathbf{L}^{(p)}\}, \{\mathbf{W}^{(p)}\}$ and $\{\mathbf{b}^{(p)}\}$ according to (18).
end for

point of the neural dynamics (14), such procedure enforces the nudged network output to be a fixed point of the free neural dynamics.

To optimize our contrastive function (17) in a stochastic (one training datum at a time) manner, we use the following procedure. For each pair of training data $\{\mathbf{r}_t^0, \mathbf{z}_t^l\}$, we run the nudged phase ($\beta \neq 0$) dynamics (14) until convergence to get the fixed point $\mathbf{r}_{\beta,t}^{(p)}$. Next, we run the free phase ($\beta = 0$) neural dynamics (14) until convergence. We collect the fixed points $\mathbf{r}_{0,t}^{(p)}$. $\mathbf{L}^{(p)}$ is updated following a gradient ascent of (15), while $\mathbf{W}^{(p)}$ and $\mathbf{b}^{(p)}$ following a gradient descent of (17):

$$\begin{aligned}\Delta \mathbf{L}^{(p)} &\propto \left(\mathbf{r}_{\beta,t}^{(p)} \mathbf{r}_{\beta,t}^{(p)\top} - \mathbf{L}^{(p)} \right), \\ \Delta \mathbf{W}^{(p)} &\propto \left(\mathbf{r}_{\beta,t}^{(p)} \mathbf{r}_{\beta,t}^{(p-1)\top} - \mathbf{r}_{0,t}^{(p)} \mathbf{r}_{0,t}^{(p-1)\top} \right), \\ \Delta \mathbf{b}^{(p)} &\propto \left(\mathbf{r}_{\beta,t}^{(p)} - \mathbf{r}_{0,t}^{(p)} \right).\end{aligned}\tag{18}$$

In practice, learning rates can be chosen differently to achieve best performance. A constant prefactor before $\mathbf{L}^{(p)}$ can be added to achieve numerical stability. The above CSM algorithm is summarized in Algorithm 1.

3.2.1 Relation to Other Energy Based Learning Algorithms

The CSM algorithm is similar in spirit to other contrastive algorithms, such as CHL and EP. Like these algorithms, CSM performs two runs of the neural dynamics in a “free” and a “nudged” phase. However there are important differences. One major difference is that in CSM, the contrast function is minimized by the feedforward weights. The lateral weights take part in maximization of a different minimax objective (15). In CHL and EP, such minimization is done with respect to all the weights.

As a consequence of this difference, the CSM algorithm uses a different update for lateral weights compared with CHL and EP algorithm. This is an anti-Hebbian

update arising from the nudged phase, and is different from EP and CHL in two ways: 1) It has the opposite sign, i.e. EP and CHL nudged/clamped phase updates are Hebbian. 2) No update is applied in the free phase. As we will demonstrate in numerical simulations, our lateral update imposes a competition between different units in the same layer. When network activity is constrained to be nonnegative, such lateral interactions are inhibitory and sparsens neural activity.

3.3 Introducing structured connectivity

We can also generalize the nudged supervised similarity matching (Eq. 11) to derive a Hebbian/anti-Hebbian network with structured connectivity. Following the idea in (Obeid et al., 2019), we can modify any of the cross terms in the layer-wise similarity matching objective (Eq. 11) by introducing synapse-specific structure constants. For example:

$$-\frac{1}{T^2} \sum_i^{N^{(p)}} \sum_j^{N^{(p-1)}} \sum_t^T \sum_{t'}^T r_{t,i}^{(p)} r_{t',i}^{(p)} r_{t,j}^{(p-1)} r_{t',j}^{(p-1)} s_{ij}^W, \quad (19)$$

where $N^{(p)}$ is the number of neurons in p -th layer, $s_{ij}^W \geq 0$ are constants that set the structure of feedforward weight matrix between p -th layer and $(p-1)$ -th layer. In particular, setting them to zero removes the connection, without changing the interpretation of energy function (Obeid et al., 2019). Similarly, we can introduce constants s_{ij}^L to specify the structure of the lateral connections (Fig. 6 A). Using such structure constants, one can introduce many different architectures, some of which we experiment with below. We present a detailed explanation of these points in the Appendix B.

4 Numerical Simulations

In this section, we report the simulation results of the CSM algorithm on a supervised classification task using the MNIST dataset of handwritten digits (LeCun et al., 2010) and CIFAR-10 image dataset. For our simulations, we used the Theano Deep Learning framework (Team et al., 2016) and modified the code released by (Scellier and Bengio, 2017). The activation functions of the units were $f(x) = \min\{1, \max\{x, 0\}\}$ and $c^{(p)} = 1/2$.

4.1 MNIST

The inputs consist of gray-scale 28 by 28 pixel-images, and each image is associated with a label ranging from $\{0, \dots, 9\}$. We encoded the labels \mathbf{z}^l as one-hot

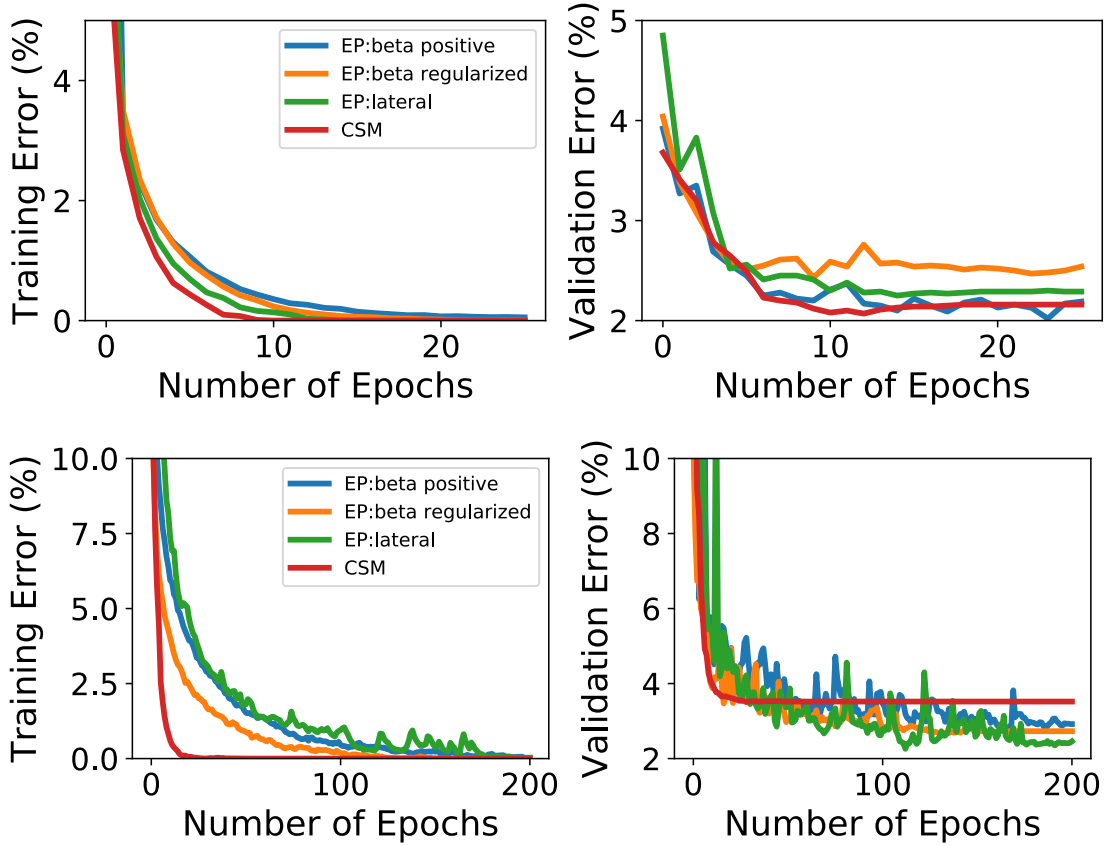


Figure 3: Comparison of training (left) and validation (right) errors between CSM and EPs algorithms for a network with one hidden layer (784-500-10, upper panels) and three hidden layers (784-500-500-500-10, lower panels).

10-dimensional vector. We trained fully connected neural networks with one and three hidden layers with lateral connections within each hidden layer. The performance of CSM algorithm was compared with several variants of EP algorithm: (1) EP: beta regularized, where randomized sign of β functions as regularization (Scellier and Bengio, 2017); (2) EP: beta positive, where β is a positive constant; (3) EP: lateral, networks with lateral connections within the same layer trained by EP, with positive constant β . In all the fully-connected network simulations for MNIST, the number of neurons in each hidden layer is 500. We attained 0% training error and 2.16% and 3.52% validation errors with CSM, in the one and three hidden layer cases respectively. This is on par with the performance of the EP algorithm, which attains a validation error of 2.53% and 2.73% respectively for variant 1 and 2.18% and 2.77% for variant 2 (Fig.3). In the 3 layer case, a training error-dependent adaptive learning rate scheme (CSM-Adaptive) was used,

wherein the learning rate for the lateral updates is successively decreased when the training error drops below certain thresholds (see Appendix C for details).

4.2 CIFAR-10

CIFAR-10 is a more challenging dataset that contains 32 by 32 RGB images of objects belonging to ten classes of animals and vehicles. For fully connected networks, the performance of CSM was compared with EP (positive constant β). We obtain validation errors of 59.21% and 48.92% in the one and two layer networks respectively in CSM, and validation errors of 57.60% and 53.43% in EP (Fig.4). The mean of the last twenty validation errors are reported here, in order to account for fluctuations about the mean. It is interesting to note that for both algorithms, the deeper network performs better for CIFAR-10, but not for MNIST. For both datasets, the best performing network trained with CSM outperforms the best performing network trained with EP. The errors corresponding to the fully connected networks for both algorithms and datasets are summarized in Table 1. Here, CSM has been compared to the variant of EP with $\beta > 0$.

Table 1: Comparison of the training and validation errors of fully connected networks for EP (beta: positive) and CSM. For both algorithms, the best performing networks correspond to two hidden layer networks for CIFAR-10 and one hidden layer networks for MNIST. Here, xHL means that the network has x hidden layers.

MNIST			CIFAR-10		
RULE	TRAIN (%)	VALIDATE (%)	RULE	TRAIN (%)	VALIDATE (%)
CSM:1HL	0.00	2.16	CSM:1HL	1.77	59.21 \pm 0.08
EP:1HL	0.03	2.18	EP:1HL	0.76	57.60 \pm 0.06
CSM:3HL	0.00	3.52	CSM:2HL	23.04	48.92 \pm 0.005
EP:3HL	0.00	2.77	EP:2HL	1.25	53.43 \pm 0.04

4.3 Neuronal Representation

Despite the similar performance of the CSM algorithm and the EP algorithm, the underlying mechanisms are different. Due to the non-negativity of hidden units and Anti-Hebbian lateral updates, lateral connections in the the CSM algorithm are inhibitory. Therefore, the learned representations are more sparse than that of the EP algorithm (Fig.5). Sparse response is a general feature of cortical neurons (Olshausen and Field, 2004) and energy-efficient, making the representations learned by CSM more biologically relevant.

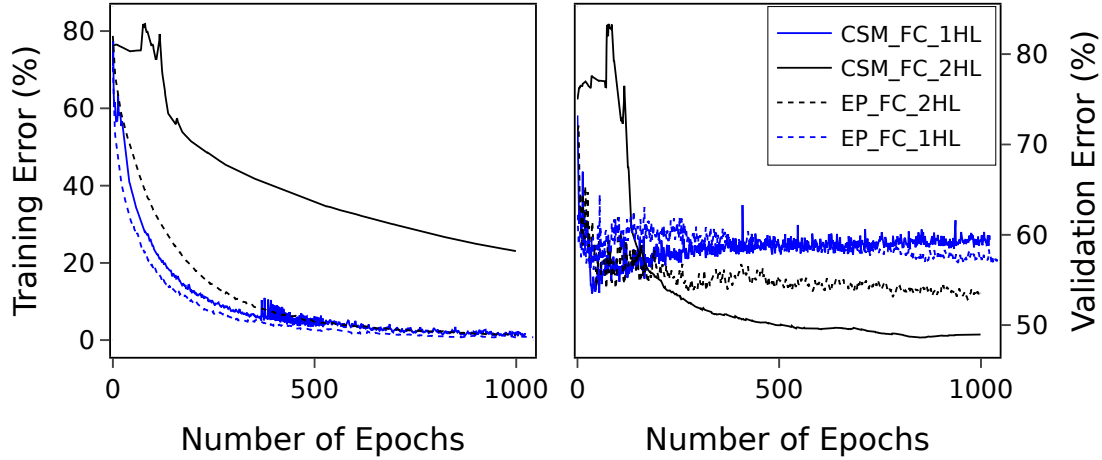


Figure 4: Training (left) and validation (right) error curves for fully connected networks trained on CIFAR-10 with CSM (solid) and EP (dotted). The best fully connected CSM network outperforms the best fully connected EP network.

4.4 Structured Networks

We also examined the performance of CSM in networks with structured connectivity. Every hidden layer can be constructed by first considering sites arranged on a two dimensional grid. Each site only receives inputs from selected nearby sites; this is controlled by the ‘radius’ parameter (Fig. 6A). This setting resembles retinotopy (Kandel et al., 2000) in the visual cortex. For each layer, several of such two dimensional grids are stacked such that multiple neurons are present at a single site; this is controlled by the ‘neurons per site’(NPS) parameter. We consider lateral connections only between neurons sharing the same (x, y) coordinate.

For MNIST dataset, networks with structured connectivity trained with the CSM rule achieved comparable performance, 2.22% validation error for a single hidden layer network with a radius of 4 and NPS of 20 (Fig. 6) (See Appendix C for details). For CIFAR-10 dataset, a one hidden layer structured network using CSM algorithm achieves 34.47% training error and 49.50% validation error after 250 epochs, which is a significant improvement compared to the fully connected one layer network. This structured network had a radius of 4 and NPS of 3. A two hidden layer structured network yielded a training error of 46.81% and a validation error of 51.36% after 250 epochs. Errors reported for the structured runs are the averages of five trials. The results for all fully connected and structured networks are reported in Appendix C and D.

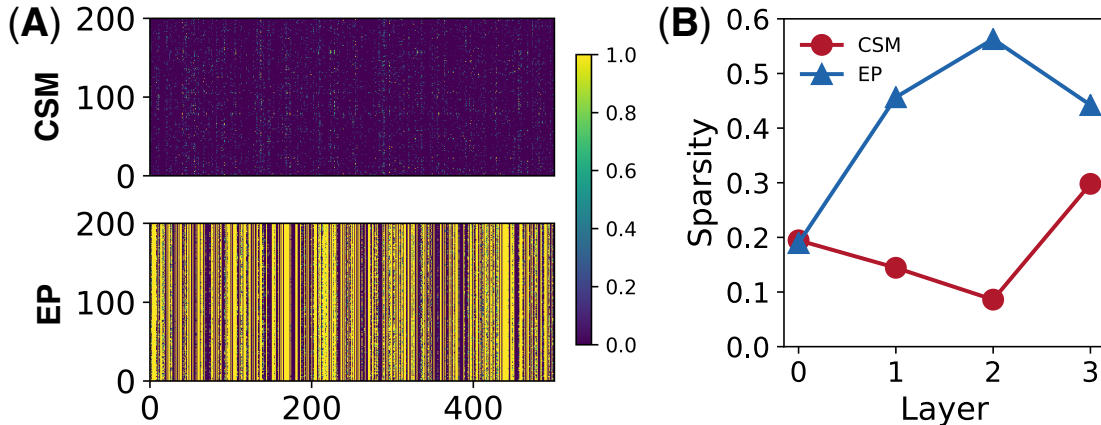


Figure 5: Representations of neurons in NNs trained by CSM algorithm is much sparser than that of EP algorithm on MNIST dataset. (A) Heatmaps of representations at the layer 2, each row is the response of 500 neurons to a given digit image. Upper: CSM algorithm. Lower: EP algorithm. (B) Representation sparsity, defined as number of neurons whose activity are larger than a threshold (0.01), along different layers. Layer 0 is the input. The network has a 784-500-500-500-10 architecture.

5 Discussion

In this paper, we proposed a new solution to the credit assignment problem by generalizing the similarity matching principle to supervised domain and proposed a biologically plausible supervised learning algorithm, the contrastive similarity matching. In CSM algorithm, supervision signal is introduced by minimizing the energy difference between a free phase and nudged phase. CSM differs significantly from other energy-based algorithms in how the contrastive function is constructed. The anti-Hebbian learning rule for the lateral connections makes the representations sparse and biological relevant. We also derived CSM for NNs with structured connectivity.

The idea of using representational similarity for training neural networks have taken various forms in previous work. The similarity matching principle has recently been used to derive various biologically plausible unsupervised learning algorithms (Pehlevan and Chklovskii, 2019), such as principal subspace projection (Pehlevan and Chklovskii, 2015), blind source separation (Pehlevan et al., 2017), feature learning (Obeid et al., 2019) and manifold learning (Sengupta et al., 2018). Recently, it has been used for semi-supervised classification (Genkin et al., 2019). Similarity matching has also been introduced as part of a local cost function to train a deep convolutional network (Nøkland and Eidnes, 2019), where instead of layer-wise similarity matching, each hidden layer aims to learn representations

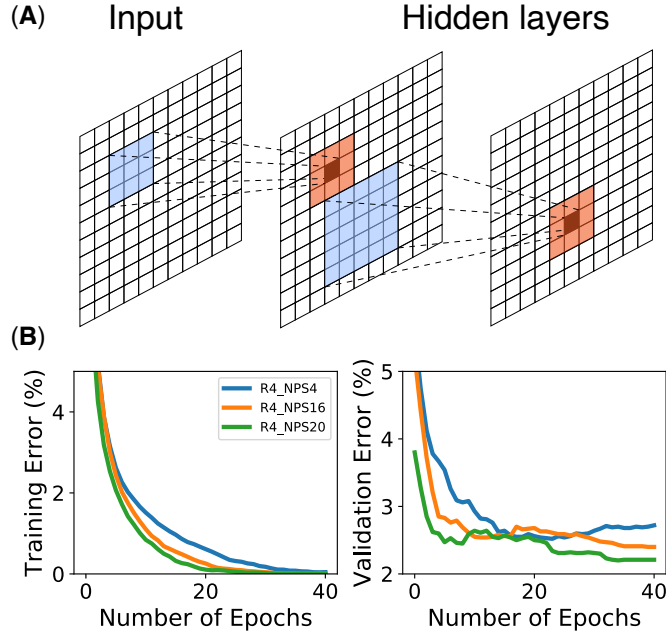


Figure 6: (A) Sketch of structured connectivity in a deep neural network. Neurons live in a 2-d grid. Each neuron takes input from a small grid (blue shades) from previous layer and a small grid of inhibition from its nearby neurons (orange shades). (B) Training and validation curves with CSM in structured on MNIST data set, single hidden layer networks, with a receptive field of radius 4 and neurons per site 4, 16 and 20.

similar to the output layer. Representational similarity matrices derived from neurobiology data has recently been used to regularize the CNNs trained on image classification. The resulting network is more robust to noise and adversarial attacks (Li et al., 2019). It would be interesting to study the robustness of NNs trained by the CSM algorithm.

A practical issue of CSM and other energy-based algorithms such as EP and CHL is that the recurrent dynamics takes a long time to converge. Recently, a discrete-time version of EP has shown much faster training speed (Ernoult et al., 2019) and the application to the CSM could be an interesting future work.

Acknowledgements

We acknowledge support by NIH and the Intel Corporation through Intel Neuro-morphic Research Community. We thank Blake Bordelon for helpful discussions.

A Supervised deep similarity matching

In this section, we follow (Obeid et al., 2019) to derive the minimax dual of deep similarity matching objective function. We start from rewriting the objective function (11) by expanding its first term and combining the same terms from adjacent layers, which gives

$$\begin{aligned} \min_{\substack{a_1 \leq \mathbf{r}_t^p \leq a_2 \\ t=1, \dots, T \\ p=1, \dots, P}} \sum_{p=1}^P \frac{\gamma^{p-P}}{2T^2} \sum_{t=1}^T \sum_{t'=1}^T \left(\mathbf{r}_t^{(p)\top} \mathbf{r}_{t'}^{(p)} \mathbf{r}_t^{(p-1)\top} \mathbf{r}_{t'}^{(p-1)} - \frac{1 + \gamma(1 - \delta_{pP})}{2} c^{(p)} \mathbf{r}_t^{(p)\top} \mathbf{r}_{t'}^{(p)} \mathbf{r}_t^{(p)\top} \mathbf{r}_{t'}^{(p)} \right) \\ + \sum_{p=1}^P \frac{2\gamma^{p-P}}{T} \sum_{t=1}^T \mathbf{F}(\mathbf{r}_t^{(p)})^\top \mathbf{1} + \frac{\beta}{T} \sum_{t=1}^T \left\| \mathbf{r}_t^{(P)} - \mathbf{z}_t^l \right\|_2^2, \end{aligned} \quad (20)$$

where $c^{(p)}$ is a parameter that change the relative importance of within-layer and between-layer similarity, we set it to be 1/2 in our numerical simulations. Plug the following identities:

$$-\frac{1}{T^2} \sum_{t=1}^T \sum_{t'=1}^T \mathbf{r}_t^{(p)\top} \mathbf{r}_{t'}^{(p)} \mathbf{r}_t^{(p-1)\top} \mathbf{r}_{t'}^{(p-1)} = \min_{\mathbf{W}^{(p)}} -\frac{2}{T} \sum_{t=1}^T \mathbf{r}_t^{(p)\top} \mathbf{W}^{(p)} \mathbf{r}_t^{(p-1)} + \text{Tr} \mathbf{W}^{(p)\top} \mathbf{W}^{(p)}, \quad (21)$$

$$\frac{1}{T^2} \sum_{t=1}^T \sum_{t'=1}^T \mathbf{r}_t^{(p)\top} \mathbf{r}_{t'}^{(p)} \mathbf{r}_t^{(p)\top} \mathbf{r}_{t'}^{(p)} = \max_{\mathbf{L}^{(p)}} \frac{2}{T} \sum_{t=1}^T \mathbf{r}_t^{(p)\top} \mathbf{L}^{(p)} \mathbf{r}_t^{(p)} - \text{Tr} \mathbf{L}^{(p)\top} \mathbf{L}^{(p)}, \quad (22)$$

in (20) and exchange the optimization order of $\mathbf{r}_t^{(p)}$ and the weight matrices, we turn the target function (11) into the following minmax problem

$$\min_{\{\mathbf{W}^{(p)}\}} \max_{\{\mathbf{L}^{(p)}\}} \frac{1}{T} \sum_{t=1}^T l_t \left(\{\mathbf{W}^{(p)}\}, \{\mathbf{L}^{(p)}\}, \mathbf{r}_t^{(0)}, \mathbf{z}_t^l, \beta \right), \quad (23)$$

where we have defined an “energy” term (Eq.13 in the main text) The neural dynamics of each layer can be derived by following the gradient of l_t :

$$\begin{aligned} \frac{d\mathbf{u}_t^{(p)}}{dt} \propto -\frac{\partial l_t}{\partial \mathbf{r}_t^{(p)}} &= 2\gamma^{p-P} \left[-\mathbf{u}^{(p)} + \mathbf{b}_t^{(p)} + \mathbf{W}^{(p)} \mathbf{r}_t^{(p-1)} + \gamma(1 - \delta_{pP}) \mathbf{W}^{(p+1)\top} \mathbf{r}_t^{(p+1)} \right. \\ &\quad \left. - [1 + \gamma(1 - \delta_{pP})] c^{(p)} \mathbf{L}^{(p)} \mathbf{r}_t^{(p)} - \beta \delta_{pP} (\mathbf{r}_t^{(P)} - \mathbf{z}_t^l) \right], \\ \mathbf{r}_t^{(p)} &= \mathbf{f}(\mathbf{u}^{(p)}). \end{aligned} \quad (24)$$

Define $\tau_p^{-1} = 2\gamma^{p-P}$, the above equation becomes Eq.14 in the main text.

B Supervised Similarity Matching for Neural Networks With Structured Connectivity

In this section, we derive the supervised similarity matching algorithm for neural networks with structured connectivity. Structure can be introduced to the quartic terms in (20):

$$-\frac{1}{T^2} \sum_i^{N^{(p)}} \sum_j^{N^{(p-1)}} \sum_t^T \sum_{t'}^T r_{t,i}^{(p)} r_{t',i}^{(p)} r_{t,j}^{(p-1)} r_{t',j}^{(p-1)} s_{ij}^{W,(p)}, \quad -\frac{1}{T^2} \sum_i^{N^{(p)}} \sum_j^{N^{(p)}} \sum_t^T \sum_{t'}^T r_{t,i}^{(p)} r_{t',i}^{(p)} r_{t,j}^{(p)} r_{t',j}^{(p)} s_{ij}^{L,(p)}, \quad (25)$$

where $s_{ij}^{W,(p)}$ and $s_{ij}^{L,(p)}$ specify the feedforward connections of layer p with $p-1$ layer and lateral connections within layer p respectively. For example, setting them to be 0s eliminates all connections. Now we have the following deep structured similarity matching cost function for supervised learning:

$$\begin{aligned} \min_{\substack{a_1 \leq \mathbf{r}_t^{(p)} \leq a_2 \\ t=1, \dots, T \\ p=1, \dots, P}} \sum_{p=1}^P \frac{\gamma^{p-P}}{2T^2} \sum_{t=1}^T \sum_{t'=1}^T \left(\mathbf{r}_t^{(p)\top} \mathbf{r}_{t'}^{(p)} \mathbf{r}_t^{(p-1)\top} \mathbf{r}_{t'}^{(p-1)} s_{ij}^{W,(p)} - \frac{1 + \gamma(1 - \delta_{pP})}{2} \mathbf{r}_t^{(p)\top} \mathbf{r}_{t'}^{(p)} \mathbf{r}_t^{(p)\top} \mathbf{r}_{t'}^{(p)} s_{ij}^{L,(p)} \right) \\ + \sum_{i=1}^P \frac{2\gamma^{p-P}}{T} \sum_{t=1}^T \mathbf{F}(\mathbf{r}_t^{(p)})^\top \mathbf{1} + \frac{\beta}{T} \sum_{t=1}^T \left\| \mathbf{r}_t^{(P)} - \mathbf{z}_t^l \right\|_2^2. \end{aligned} \quad (26)$$

For each layer, we can define dual variables for $\mathbf{W}_{ij}^{(p)}$ and $\mathbf{L}_{ij}^{(p)}$ for interactions with positive constants, and define the following variables

$$\bar{W}_{ij}^{(p)} = \begin{cases} W_{ij}^{(p)}, & s_{ij}^{W,(p)} \neq 0 \\ 0, & s_{ij}^{W,(p)} = 0 \end{cases}, \quad \bar{L}_{ij}^{(p)} = \begin{cases} L_{ij}^{(p)}, & s_{ij}^{L,(p)} \neq 0 \\ 0, & s_{ij}^{L,(p)} = 0 \end{cases} \quad (27)$$

Now we can rewrite (26) as:

$$\min_{\{\bar{\mathbf{W}}^{(p)}\}} \max_{\{\bar{\mathbf{L}}^{(p)}\}} \frac{1}{T} \sum_{t=1}^T \bar{l}_t \left(\{\bar{\mathbf{W}}^{(p)}\}, \{\bar{\mathbf{L}}^{(p)}\}, \mathbf{r}_t^{(0)}, \mathbf{z}_t^l, \beta \right), \quad (28)$$

where

$$\begin{aligned} \bar{l}_t := \min_{\substack{a_1 \leq \mathbf{r}_t^{(p)} \leq a_2 \\ p=1, \dots, P}} \sum_{p=1}^P \gamma^{p-P} \left\{ \sum_{\substack{i,j \\ s_{ij}^{W,(p)} \neq 0}} W_{ij}^{(p)^2} - \sum_{\substack{i,j \\ s_{ij}^{L,(p)} \neq 0}} \frac{1 + \gamma(1 - \delta_{pP})}{s_{ij}^{L,(p)}} L_{ij}^{(p)^2} \right. \\ \left. + [1 + \gamma(1 - \delta_{pP})] \mathbf{r}_t^{(p)\top} \mathbf{L}^{(p)} \mathbf{r}_t^{(p)} - 2\mathbf{r}_t^{(p)\top} \mathbf{W}^{(p)} \mathbf{r}_t^{(p-1)} + 2\mathbf{F}(\mathbf{r}_t^{(p)})^\top \right\} + \beta \left\| \mathbf{r}_t^{(P)} - \mathbf{z}_t^l \right\|_2^2. \end{aligned} \quad (29)$$

The neural dynamics follows the gradient of (29), which is

$$\begin{aligned}\tau_p \frac{d\mathbf{u}_t^{(p)}}{dt} &= -\mathbf{u}^{(p)} + \mathbf{b}_t^{(p)} + \bar{\mathbf{W}}^{(p)} \mathbf{r}_t^{(p-1)} + \gamma(1 - \delta_{pP}) \bar{\mathbf{W}}^{(p+1)\top} \mathbf{r}_t^{(p+1)} - [1 + \gamma(1 - \delta_{pP})] \bar{\mathbf{L}}^{(p)} \mathbf{r}_t^{(p)} \\ &\quad - \beta \delta_{pP} (\mathbf{r}_t^{(P)} - \mathbf{z}_t^l), \\ \mathbf{r}_t^{(p)} &= \mathbf{f}(\mathbf{u}^{(p)}), \quad p = 1, \dots, P.\end{aligned}\tag{30}$$

Local learning rules follow the gradient descent and ascent of (29):

$$\Delta W_{ij}^{(p)} \propto \left(r_j^{(p)} r_i^{(p-1)} - \frac{W_{ij}^{(p)}}{s_{ij}^{W,(p)}} \right), \tag{31}$$

$$\Delta L_{ij}^{(p)} \propto \left(r_j^{(p)} r_i^{(p)} - \frac{L_{ij}^{(p)}}{s_{ij}^{L,(p)}} \right). \tag{32}$$

C Hyperparameters and Performance in Numerical Simulations with the MNIST Dataset

C.1 One Hidden Layer

The models were trained until the training error dropped to 0% or as close to 0% as possible (as in the case of EP algorithm with $\beta > 0$); errors reported herein correspond to errors obtained for specific runs and do not reflect ensemble averages. The training and validation errors below, and in subsequent subsections are reported at an epoch when the training error has dropped to 0%, or at the last epoch for the run (eg. for EP $\beta > 0$). This epoch number is recorded in the last column.

C.2 Three Hidden Layers

In Table 2, the CSM algorithm employs a scheme with decaying learning rates. Specifically, the learning rates for lateral updates are divided by a factor of 5, 10, 50, and 100 when the training error dropped below 5%, 1%, 0.5%, and 0.1% respectively.

C.3 Structured Connectivity

In this section, we explain the simulation for structured connectivity and report the results. Every hidden layer in these networks can be considered as multiple two dimensional grids stacked onto each other, with each grid containing neurons/units

Table 2: Comparison of the training and validation errors of different algorithms for one hidden layer NNs on MNIST data set

ALGORITHM	LEARNING RATE	TRAINING ERROR (%)	VALIDATION ERROR (%)	No. EPOCHS
EP: $\pm\beta$	$\alpha_W = 0.1, 0.05$	0	2.53	40
EP: $+\beta$	$\alpha_W = 0.5, 0.125$	0.034	2.18	100
EP: LATERAL	$\alpha_W = 0.5, 0.25, \alpha_L$ $= 0.75$	0	2.29	25
CSM	$\alpha_W = 0.5, 0.375,$ $\alpha_L = 0.01$	0	2.16	25

at periodically arranged sites. Each site only receives inputs from selected nearby sites. In this scheme, we consider lateral connections only between neurons sharing the same (x, y) coordinate, and the length and width of the grid are the same. In the table below, ‘Full’ refers to simulations where the input is the 28×28 MNIST input image and ‘Crop’ refers to simulations in which the input image is a cropped 20×20 MNIST image. The first three, annotated by ‘Full’, correspond to the simulations reported in the main text. Errors are reported at the last epoch for the run. In networks with structural connectivity, additional hyperparameters are required to constrain the structure, which as enumerated below:

- Neurons-per-site (nps): The number of neurons placed at each site in a given hidden layer, i.e. the number of two dimensional grids stacked onto each other. The nps for the input is 1.
- Stride: Spacing between adjacent sites, relative to the input channel. The stride of the input is always 1, i.e. sites are placed at (0, 0), (0, 1), (1, 0), so on, on the two dimensional grid. If the stride of the l -th layer is s , the nearest sites to the site at the origin will be (0, s) and (s , 0). The stride increases deeper into the network. Specifying the stride also determines the dimension of the grid. A layer with stride s and nps n , will have $d \times d \times n$ units, where $d = 28/s$ for the ‘Full’ runs and $d = 20/s$ for the ‘Crop’ runs. The nps values and stride together assign coordinates to all the units in the network.
- Radius: The radius of the circular two-dimensional region that all units in the previous layer must lie within in order to have non-zero weights to the current unit. Any units in the previous layer, lying outside the circle will not be connected to the unit.

Table 3: Comparison of the training and validation errors of different algorithms for three hidden layer NNs on MNIST data set

ALGORITHM	LEARNING RATE	TRAINING ERROR (%)	VALIDATION ERROR (%)	NO. EPOCHS
EP: $\pm\beta$	$\alpha_W=0.128, 0.032, 0.008, 0.002$	0	2.73	250
EP: $+\beta$	$\alpha_W=0.128, 0.032, 0.008, 0.002$	0	2.77	250
EP LATERAL	$\alpha_W=0.128, 0.032, 0.008, 0.002$; $\alpha_L=0.192, 0.048, 0.012$	0	2.4	250
CSM	$\alpha_W=0.5, 0.375, 0.281, 0.211$; $\alpha_L=0.75, 0.562, 0.422$	0	4.82	250
CSM ADAP- TIVE	$\alpha_W=0.5, 0.375, 0.281, 0.211$; $\alpha_L=0.75, 0.562, 0.422$	0	3.52	250

Table 4: Comparison of the training and validation errors of different algorithms for one hidden layer NNs with structured connectivity on MNIST data set

ALGORITHM	LEARNING RATE	TRAINING ERROR (%)	VALIDATION ERROR (%)	NO. EPOCHS
R4, NPS4, FULL	$\alpha_W=0.5, 0.375$; $\alpha_L=0.01$	0.02	2.71	50
R4, NPS16, FULL	$\alpha_W=0.5, 0.25$; $\alpha_L=0.75$	0	2.41	49
R4, NPS20, FULL	$\alpha_W=0.664, 0.577$; $\alpha_L=0.9$	0	2.22	50
R8, NPS80, CROP	$\alpha_W=0.664, 0.577$; $\alpha_L=0.9$	0.01	2.27	20
R4, NPS4, CROP	$\alpha_W=0.099, 0.065$; $\alpha_L=0.335$	0.08	2.98	100
R8, NPS4, CROP	$\alpha_W=0.099, 0.065$; $\alpha_L=0.335$	0	2.73	100
R8, NPS20, CROP	$\alpha_W=0.664, 0.577$; $\alpha_L=0.9$	0	2.23	79

D Hyperparameters and Performance in Numerical Simulations with the CIFAR-10 Dataset

The validation error column for Fully Connected runs reports the average of the last twenty validation errors reported at the end of the training period. For the Structured runs, the training and validation errors reported are the average of the last epoch’s reported errors from 5 trials. This is done in order to account for fluctuations in the error during training.

Table 5: Comparison of the validation errors of different algorithms for different networks.

ALGORITHM, CONNECTIVITY, NO. HIDDEN LAYERS	LEARNING RATE	TRAIN ERROR (%)	VAL ERROR (%)	NO. EPOCHS
CSM, FC, 1HL	$\alpha_W = 0.059, 0.017$ $\alpha_L = 0.067$	1.77	59.21 ± 0.08	1000
CSM, FC, 2HL	$\alpha_W =$ $0.018, 7.51 \times 10^{-4}, 3.07 \times 10^{-5}$ $\alpha_L = 0.063, 2.59 \times 10^{-3}$	23.04	48.92 ± 0.005	1000
CSM, STR, 1HL	$\alpha_W = 0.050, 0.0375$ $\alpha_L = 0.01$	$34.47 \pm$ 3.66	49.50 ± 0.66	250
CSM, STR, 2HL	$\alpha_W = 0.265, 0.073, 0.020$ $\alpha_L = 0.075, 0.020$	$46.81 \pm$ 0.61	51.36 ± 0.71	250
EP, FC, 1HL	$\alpha_W = 0.014, 0.011$	0.75	57.60 ± 0.06	1000
EP, FC, 2HL	$\alpha_W = 0.014, 0.011, 1.25$	1.25	53.43 ± 0.04	1000

References

- Belilovsky, E., Eickenberg, M., and Oyallon, E. (2018). Greedy layerwise learning can scale to imagenet. *arXiv preprint [arXiv:1812.11446](https://arxiv.org/abs/1812.11446)*.
- Crick, F. (1989). The recent excitement about neural networks. *Nature*, 337(6203):129–132.
- Ernoul, M., Grollier, J., Querlioz, D., Bengio, Y., and Scellier, B. (2019). Updates of equilibrium prop match gradients of backprop through time in an rnn with static input. In *Advances in Neural Information Processing Systems*, pages 7079–7089.
- Genkin, A., Sengupta, A. M., and Chklovskii, D. (2019). A neural network for semi-supervised learning on manifolds. In *International Conference on Artificial Neural Networks*, pages 375–386. Springer.
- Grill-Spector, K. and Weiner, K. S. (2014). The functional architecture of the ventral temporal cortex and its role in categorization. *Nature Reviews Neuroscience*, 15(8):536–548.
- Guerguiev, J., Lillicrap, T. P., and Richards, B. A. (2017). Towards deep learning with segregated dendrites. *ELife*, 6:e22901.
- Hinton, G. E. and McClelland, J. L. (1988). Learning representations by recirculation. In *Neural information processing systems*, pages 358–366.
- Kandel, E. R., Schwartz, J. H., Jessell, T. M., of Biochemistry, D., Jessell, M. B. T., Siegelbaum, S., and Hudspeth, A. (2000). *Principles of neural science*, volume 4. McGraw-hill New York.
- LeCun, Y., Cortes, C., and Burges, C. (2010). Mnist handwritten digit database. *ATT Labs [Online]*. Available: <http://yann.lecun.com/exdb/mnist>, 2.
- Lee, D.-H., Zhang, S., Fischer, A., and Bengio, Y. (2015). Difference target propagation. In *Joint European Conference on Machine Learning and Knowledge Discovery in Databases*, pages 498–515. Springer.
- Li, Z., Brendel, W., Walker, E., Cobos, E., Muhammad, T., Reimer, J., Bethge, M., Sinz, F., Pitkow, Z., and Tolias, A. (2019). Learning from brains how to regularize machines. In *Advances in Neural Information Processing Systems*, pages 9525–9535.

- Lillicrap, T. P., Cownden, D., Tweed, D. B., and Akerman, C. J. (2016). Random synaptic feedback weights support error backpropagation for deep learning. *Nature Communications*, 7:13276.
- Lillicrap, T. P., Santoro, A., Marris, L., Akerman, C. J., and Hinton, G. (2020). Backpropagation and the brain. *Nature Reviews Neuroscience*, pages 1–12.
- Movellan, J. R. (1991). Contrastive hebbian learning in the continuous hopfield model. In *Connectionist models*, pages 10–17. Elsevier.
- Nøkland, A. (2016). Direct feedback alignment provides learning in deep neural networks. In *Advances in Neural Information Processing Systems*, pages 1037–1045.
- Nøkland, A. and Eidnes, L. H. (2019). Training neural networks with local error signals. *arXiv preprint [arXiv:1901.06656](https://arxiv.org/abs/1901.06656)*.
- Obeid, D., Ramambason, H., and Pehlevan, C. (2019). Structured and deep similarity matching via structured and deep hebbian networks. In *Advances in Neural Information Processing Systems*, pages 15377–15386.
- Olshausen, B. A. and Field, D. J. (2004). Sparse coding of sensory inputs. *Current opinion in neurobiology*, 14(4), 481–487.
- Ororbia, A. G. and Mali, A. (2019). Biologically motivated algorithms for propagating local target representations. In *Proceedings of the AAAI Conference on Artificial Intelligence*, volume 33, pages 4651–4658.
- Pehlevan, C. and Chklovskii, D. (2015). A normative theory of adaptive dimensionality reduction in neural networks. In *Advances in neural information processing systems*, pages 2269–2277.
- Pehlevan, C. and Chklovskii, D. B. (2019). Neuroscience-inspired online unsupervised learning algorithms: Artificial neural networks. *IEEE Signal Processing Magazine*, 36(6):88–96.
- Pehlevan, C., Mohan, S., and Chklovskii, D. B. (2017). Blind nonnegative source separation using biological neural networks. *Neural computation*, 29(11):2925–2954.
- Pehlevan, C., Sengupta, A. M., and Chklovskii, D. B. (2018). Why do similarity matching objectives lead to hebbian/anti-hebbian networks? *Neural computation*, 30(1):84–124.

- Richards, B. A. and Lillicrap, T. P. (2019). Dendritic solutions to the credit assignment problem. *Current Opinion in Neurobiology*, 54:28–36.
- Rumelhart, D. E., Hinton, G. E., and Williams, R. J. (1986). Learning representations by back-propagating errors. *nature*, 323(6088):533–536.
- Sacramento, J., Costa, R. P., Bengio, Y., and Senn, W. (2018). Dendritic cortical microcircuits approximate the backpropagation algorithm. In *Advances in Neural Information Processing Systems*, pages 8721–8732.
- Scellier, B. and Bengio, Y. (2017). Equilibrium propagation: Bridging the gap between energy-based models and backpropagation. *Frontiers in computational neuroscience*, 11:24.
- Sengupta, A., Pehlevan, C., Tepper, M., Genkin, A., and Chklovskii, D. (2018). Manifold-tiling localized receptive fields are optimal in similarity-preserving neural networks. In *Advances in Neural Information Processing Systems*, pages 7080–7090.
- Team, T. T. D., Al-Rfou, R., Alain, G., Almahairi, A., Angermueller, C., Bahdanau, D., Ballas, N., Bastien, F., Bayer, J., Belikov, A., et al. (2016). Theano: A python framework for fast computation of mathematical expressions. *arXiv preprint [arXiv:1605.02688](https://arxiv.org/abs/1605.02688)*.
- Whittington, J. C. and Bogacz, R. (2017). An approximation of the error back-propagation algorithm in a predictive coding network with local hebbian synaptic plasticity. *Neural Computation*, 29(5):1229–1262.
- Whittington, J. C. and Bogacz, R. (2019). Theories of error back-propagation in the brain. *Trends in cognitive sciences*.
- Xie, X. and Seung, H. S. (2003). Equivalence of backpropagation and contrastive hebbian learning in a layered network. *Neural computation*, 15(2):441–454.